HHS Public Access

Author manuscript

Synapse. Author manuscript; available in PMC 2015 March 04.

Published in final edited form as:

Synapse. 2012 July ; 66(7): 608–621. doi:10.1002/syn.21547.

Role of perisynaptic parameters in neurotransmitter homeostasis - computational study of a general synapse

Sandeep Pendyam[1], **Ashwin Mohan**[1], **Peter W. Kalivas**[2], and **Satish S. Nair**[1,*]

[1]Department of Electrical and Computer Engineering, University of Missouri, Columbia, Missouri

[2]Department of Neurosciences, Medical University of South Carolina, Charleston, South Carolina

Abstract

Extracellular neurotransmitter concentrations vary over a wide range depending on the type of neurotransmitter and location in the brain. Neurotransmitter homeostasis near a synapse is achieved by a balance of several mechanisms including vesicular release from the presynapse, diffusion, uptake by transporters, non-synaptic production, and regulation of release by autoreceptors. These mechanisms are also affected by the glia surrounding the synapse. However, the role of these mechanisms in achieving neurotransmitter homeostasis is not well understood. A biophysical modeling framework was proposed to reverse engineer glial configurations and parameters related to homeostasis for synapses that support a range of neurotransmitter gradients. Model experiments reveal that synapses with extracellular neurotransmitter concentrations in the micromolar range require non-synaptic neurotransmitter sources and tight synaptic isolation by extracellular glial formations. The model was used to identify the role of perisynaptic parameters on neurotransmitter homeostasis, and to propose glial configurations that could support different levels of extracellular neurotransmitter concentrations. Ranking the parameters based on their effect on neurotransmitter homeostasis, non-synaptic sources were found to be the most important followed by transporter concentration and diffusion coefficient.

Keywords

computational model; neurotransmitter homeostasis; glial configurations; non-synaptic sources; synapse

INTRODUCTION

Maintenance of accurate levels of *in vivo* extracellular neurotransmitter concentration is critical for several neurological processes such as migration and differentiation of brain cells during development (LoTurco et al., 1995; Nguyen et al., 2001; Manent and Represa, 2007) and for synaptic plasticity (Featherstone and Shippy, 2008). For monoamine-, acetylcholine- and purine- type neurotransmitters, extracellular concentrations are maintained by synaptic release and are usually at low levels (< 100 nM; Trommershauser et al., 2003). On the other hand, amino acid-type neurotransmitters, such as glutamate and GABA, have synaptic and

[*]**Correspondence may be sent to:** Satish S. Nair, Ph.D., Electrical and Computer Engineering, University of Missouri, Columbia, MO, 65211, Tel: 573-882-2964, Fax: 573-882-0397, nairs@missouri.edu.

non-synaptic sources (Reissner and Kalivas, 2010) to maintain higher extracellular concentration levels. Recent reports suggest that non-synaptic extracellular neurotransmitter concentration influences synaptic signaling (Kalivas, 2009; Reissner and Kalivas, 2010). For the case of glutamate, based on the measuring technique and the brain region, estimates of the extracellular concentrations reported vary from 25 nM (Herman and Jahr, 2007) to 5μM (Bouvier et al., 1992; Baker et al., 2003; Nyitrai et al., 2006; Day et al., 2006). Several mechanisms, including neurotransmitter diffusion into the perisynaptic space (defined as the cleft and region near the synapse) after release, binding/uptake by transporters present on glial sheaths, non-synaptic production of neurotransmitters and activation of autoreceptors that regulate release, are responsible for maintaining neurotransmitter concentration within certain ranges (homeostasis) in the perisynaptic and extracellular regions. The existence of numerous nonlinear mechanisms makes the characterization of homeostasis difficult for such synapses. This motivated the development of a computational model to provide insights related to homeostatic conditions for synapses which supported gradients in neurotransmitter concentrations between the synaptic cleft and the extracellular space (referred to hereafter as 'neurotransmitter gradients'). Here, we propose a computational model for a general synapse and neurotransmitter, that is applicable for any extracellular concentration level.

Previous modeling studies related to glutamate have focused on neurotransmitter time courses in the synapse based on receptor (AMPA/NMDA) activation (Clements, 1996; Diamond and Jahr, 1997) and on determining the accessibility of synaptically released glutamate to the extracellular space by considering diffusion out of the synapse and elimination by glutamate transporters (Rusakov and Kullman, 1998; Rusakov, 2001; Barbour, 2001; Franks et al., 2002; Diamond, 2005). While these models established guidelines for neurotransmitter profiles and time courses, they did not focus on possible glial configurations and parameters that controlled perisynaptic and extracellular neurotransmitter levels under homeostatic conditions in presence of both synaptic and non-synaptic neurotransmitter sources.

Pendyam et al., (2009) reported a computational model of glutamate homeostasis in the cortico-accumbens synapse incorporating the mechanisms cited. The model provided a specific glial configuration that supported gradients in glutamate concentration observed after chronic cocaine. The present study utilized the computational framework to develop other possible glial configurations for a general class of synapses. We considered a cortico-accumbens glutamatergic example case synapse, and asked - What glial configuration can support neurotransmitter gradients during normal synaptic functioning without desensitizing synaptic receptors. How do perisynaptic parameters such as diffusion, transporter density and distribution, molecules per release, and non-synaptic production rate, affect homeostasis around a synapse? The insights gained from such a reverse engineering approach can then be used to predict glial configurations for a general class of synapses that support neurotransmitter gradients.

METHODS

An example case of a cortico-accumbens synapse was used to illustrate the proposed computational framework. We developed a continuous finite-element partial-differential equation model to simulate diffusion in an idealized volume surrounding a glutamatergic cortico-accumbens synapse. The model was developed using C++ software (Microsoft Visual Studio 2005, WA, USA), and an integration time step of 0.5 μs was used. The model was simulated for a total of 6 seconds to achieve homeostasis. Each model experiment took 30 minutes on Linux based cluster.

Model inputs and baseline parameters

Baseline physiological parameters for the example case cortico-accumbens synapse were obtained as reported in the literature.

Molecules per release and firing frequency—Each action potential (resulting from the firing frequency and release probability) in the simulated model resulted in an instantaneous vesicular release into the cleft. The molecules per release for glutamatergic synapses were in the range 4,700–10,000 (Bruns and Jahn, 1995), and this was the range used in the study (table 1). For the glutamatergic cortico-accumbens synapse considered, basal presynaptic firing frequency ranges from 1–3 Hz (Trantham et al., 2002), with burst frequencies reaching up to 15 Hz (high frequency state; Chang et al., 1997; Peters et al., 2005; Sun and Rebec, 2006).

Presynaptic regulation of release probability—Release probability is regulated following the stimulation of presynaptic autoreceptors (e.g., mGluR2/3- glutamate; $GABA_B$-GABA; and D_2- dopamine; Squire et al., 2002; Dietrich et al., 2002; Losonczy et al., 2003; Billups et al., 2005) which are located outside the synaptic cleft (Alagarsamy et al., 2001). The average synaptic release probability typically ranges from 0.1–0.5, with maximum release probability estimate for cortico-accumbens synapse being at ~ 0.4 (Ding et al., 2008). Using *in vivo* microdialysis it has been shown that blocking mGluR2/3 elevates extracellular concentrations of glutamate (Xi et al., 2002; Wolf, 2010) indicating that partial tone exists on mGluR2/3 regulating glutamate release. In the proposed model, presynaptic tone on mGluR2/3 was computed as release probability. GTPγS binding revealed that G protein signaling by stimulating mGluR2/3 increased as a logarithm of agonist dose (Xi et al., 2002) and hence, the relationship between release probability and autoreceptor occupancy was modeled as a logarithmic function. Using this, the autoreceptor function for mGluR2/3 was modeled as a change in release probability between 0.08 (100% occupancy) and 0.4 (0% occupancy; max. release probability; table 1). The basal level of glutamate in the vicinity of perisynaptic mGluR2/3 was adjusted in the present model to produce ~50% occupancy (release probability of 0.14; Billups et al., 2005) based upon the range of dissociation constant (k_d) values reported for the receptor (0.1–0.3 μM; Schoepp and True, 1992).

Diffusion—Diffusion is non-homogenous and anisotropic in the extracellular space. The size and irregular geometry of the diffusion channels differ substantially around individual

cells and this directs the movement of several neuroactive substances in the extracellular space (Sykova, 2004). Diffusion in the extracellular space is typically characterized by volume fraction α (void space/total tissue volume) and tortuosity λ (hindrance to diffusion imposed by local boundaries or local viscosity; Murthy and Sejnowski, 1997). Volume fraction a in brain tissue is estimated to be around 0.2 (Nicholson and Sykova, 1998). Tortuosity λ is estimated to be 1.2–2.4 based on diffusion measurements over a range of 100–300 μm (Nicholson, 2001). Tortuosity is a composite parameter that contains a significant geometrical component, although other factors such as interstitial viscosity may contribute to it (Tao et al., 2005). A lower diffusion coefficient than water (<1 μm^2/ms) is attributed to the microscopic viscous drag on the diffusing molecule at atomically fine spatial scales. This would include molecule interactions with proteins and microfilaments in the ECS. The additional interactions that the molecules have with larger scale diffusion barriers such as spines, small axonal boutons and glia fall under geometric tortuosity. This is not accounted for in the diffusion coefficient, (D). A microscopic diffusion coefficient in the range 0.05–0.41 μm^2/ms (Saftenku, 2005) was considered.

Transporters—Neurotransmitter concentration in the perisynaptic region is controlled by high density transporters present on the glia (e.g., for glutamate and GABA) or on the presynapse (e.g., for dopamine, norepinephrine, and serotonin; Squire et al., 2002). These transporters eliminate excess neurotransmitter diffusing out of the cleft and maintain appropriate concentrations (Tanaka et al., 1997; Danbolt, 2001) preventing excitotoxicity. The glial membranes that are closest to the synapse have a higher expression of transporters (Cholet et al., 2002) with larger numbers on the postsynaptic side (Lehre and Rusakov, 2002). Glutamate transporters (EAATs - GLAST and GLT; collectively termed XAG) are present on glial membranes (Danbolt, 2001) with surface densities ranging from 2,500–10,000 molecules/μm^2.

Non-synaptic neurotransmitter sources—As noted earlier, the extracellular composition of glutamate is derived from both synaptic and non-synaptic sources (van der Zeyden, 2008). Different types of non-synaptic sources of glutamate (e.g., cystine glutamate exchanger, xc-; Baker et al., 2003; Bridges, 2011) contribute to the extracellular neurotransmitter concentration. Wyatt et al., (1996) estimated the exchange rate for xc- system to be 450 μmol $l^{-1}hr^{-1}$ based on cerebellar slices (density of xc- is higher in the cortex by a factor of 2.4; Warr et al., 1999).The increase in glutamate concentration in the extracellular space (with a volume fraction 0.12) would be at a rate of 450*2.4/ (0.12) μM $hr^{-1=}$ 9 mM hr^{-1}. Since extracellular concentration in accumbens is two fold higher than that in the cortex (Baker et al., 2003), we assumed xc- resulted in production rates between 10–55 mM hr^{-1} in the accumbens.

Framework for modeling a class of synapses

Based on electron micrograph studies of perisynaptic environment of hippocampal area CA1 (Rusakov and Kullman, 1998), Rusakov, (2001) proposed a mathematical modeling framework. Figure 1 represents a 2D schematic of model. The 3D model can be reconstructed by rotating the 2D schematic along the axis perpendicular to the cleft. The perisynaptic environment in the model consisted of two rigid hemispheres representing the

pre- and post- terminals of the synapse (see figure 1), with radius r = 160 nm, and a separation of δ =20 nm (synaptic cleft; Rusakov and Kullman, 1998; Rusakov, 2001; Diamond, 2005). Around this synapse were 40 concentric 25 nm thick spherical shell compartments (i_1– i_{40}) resulting in the outer boundary of the perisynaptic region modeled being at a distance of 1 μm from the edge of the synapse. Each shell was divided into 9 compartments (20° angle increments, j_1–j_9) circumferentially, permitting XAG and xc- concentrations to be assigned individually to each compartment of any shell. For the outermost shell, e.g., i = 40, the boundary condition of flux = 0 was imposed at the outer edge of all compartments, to simulate identical neighboring synapses. That is, no flux entered or left the outer boundary of this shell.

Glial coverage—Based on computer-assisted three-dimensional reconstructions of five different central excitatory synapses, Rollenhagen and Lubke, (2006) have shown that glial processes are in close proximity to nerve terminals. They reported notable differences with respect to the ensheathing of the synaptic complex by glial processes depending on the brain region, with coverage varying between 8 – 90%. Certain synapses are tightly ensheathed by glial processes (Sykova, 2004), for example, cortical input synapses that are completely isolated from the surrounding neuropil, and close to 90% of cerebellar synapses are ensheathed. Also, some synapses have little glial ensheathment, e.g., hippocampal mossy fiber-CA3 synapses.

Due to the large (4–5 μM) extracellular neurotransmitter concentration for our example cortico-accumbens synapse, we considered multiple glial sheaths, i.e., tighter ensheathment of the synapse. However, lower extracellular neurotransmitter concentrations require far less glial coverage as described in ‘Results’. The glial environment modeled is a geometric equivalent of the hindrance to molecules offered by dendritic spines, small axonal boutons and glia. The thickness of glial sheath was reported as 100 nm (Rusakov, 2001) to reflect the minimum width of glial profiles observed in electron micrographs. In the proposed model, glial structures were created by volume populating XAG and xc- in the spherical shells surrounding the synapse. Two concentric shells (G_{iA} and G_{iB}; i = 1 to 3; see figure 1) were combined to form a glial sheath (of 50 nm thickness) with the surface between them modeled as impermeable, i.e., flux across this surface is zero. The individual glial sheath (G_i in figure 1) structure was akin to that previously reported in the literature (Rusakov, 2001; Pendyam et al., 2009; Mohan et al., 2010), but the configuration itself is different (figure 1) in its orientation, placement and number of glial folds. The non-synaptic release sites, xc-, were modeled as being located on the outer surface of the glial sheath G_3 (Mohan et al., 2010). Beyond G_3 (at a distance of 0.225 μm from the edge of the synapse), a porous ECS without any XAG or xc- was modeled. For the configuration reported in figure 1, the glial environment occupied ~13% of total neuropil volume.

Model equations—The mathematical equations were the standard conservation and flux equations described in Pendyam et al. (2009). Also, see Rusakov, (2001) for a comprehensive description including derivations). A mass balance for glutamate in each compartment yields Eqn.1 (Rusakov, 2001),

$$[Glu]_t = [Glu]_{t-dt} + (\Sigma(J_R)S_R + \Sigma(J_T)S_T)\frac{dt}{V} + (v_+ - v_-) \quad (1)$$

Where [*Glu*] represents the concentration of glutamate in a compartment, S_R is the surface area between adjacent volume elements in the radial direction, and S_T is the surface area shared by adjacent volume elements in the tangential direction. The radial and tangential fluxes into the compartment are denoted by J_R and J_T respectively. Each compartment has a volume of *V*. The term v_+ accounts for the production of glutamate by the xc- and unbinding of glutamate from the transporters, while the term v_- accounts for reduction in glutamate due to transporter binding. The glutamate flux *J* between adjacent volume elements A and B is computed by Eqn. 2,

$$J_{AB}(t) = -D\nabla[Glu] = -\frac{D}{ds}([Glu]_{A,t-dt} - [Glu]_{B,t-dt}) \quad (2)$$

where $[Glu]_A$ and $[Glu]_B$ represent concentration of glutamate in compartment A and B respectively, D is the diffusion constant, *ds* is the spatial distance between compartment centroids. For each compartment, this flux is calculated considering the two other compartments connected to it radially, and the two connected in the tangential direction. We monitored the glutamate flux at the edge of the outermost glial sheath (G_3 in configuration 1) to measure its magnitude and direction, since this would help determine the influence of non-synaptic glutamate on synaptic receptors, as well as the effect of synaptic release on extracellular concentration.

The final set of transporter kinetic equations for each compartment, is given by Eqn. 3,

$$\begin{aligned}
&[Glu]_t = [Glu]_{t=dt} + (-k_1[Glu]_{t-dt}[XAG]_{t-dt} + k_{-1}[Glu-XAG]_{t-dt})dt \\
&[Glu-XAG]_t = [Glu-XAG]_{t-dt} + \{-(k_{-1}+k_2)[Glu-XAG]_{t-dt} + k_1[Glu]_{t-dt}[XAG]_{t-dt}\}dt \\
&[Glu-XAG]_t + [XAG]_t = [Glu-XAG]_{t-dt} + [XAG]_{t-dt} = [XAG_{total}] \\
&[Glu_{in}]_t = [Glu_{in}]_{t-dt} + k_2 * [Glu-XAG]_{t-dt} * dt
\end{aligned} \quad (3)$$

Where [*XAG*] and [*Glu-XAG*] represents the compartmental concentrations of transporter and the bound complex, respectively, and [Glu_{in}] represents the uptake by XAG. The kinetics for XAG $k_1 = 10^4\ M^{-1}\ ms^{-1}$, $k_{-1} = 0.2\ ms^{-1}$, and $k_2 = 0.1\ ms^{-1}$ were taken from Rusakov, (2001), Lehre and Rusakov, (2002) which were based on physiology (Bergles and Jahr, 1994).

Model constraints—The simulated model was validated by satisfying transient and steady state values obtained experimentally (i) Transient synaptic conditions conforming to reported transmitter decay time course e.g., for glutamate as in (Clements et al., 1992; Tong and Jahr, 1994; Clements, 1996; Diamond and Jahr, 1997) (ii) Steady state synaptic concentrations which need to be low to avoid receptor excitotoxicity (e.g., ~100 nM for glutamate; Patneau and Mayer, 1990) and (iii) Steady state extracellular concentrations (e.g., glutamate basal concentrations are in the range 5.6 ± 1 μM for the cortico-accumbens example case; Baker et al., 2003; Sun and Rebec, 2006) with presynaptic stimulation (both low and high frequency cases). The experimentally defined basal (1–3 Hz) and high

frequency (12–15 Hz) concentrations of extracellular glutamate were modeled as being at the point P_{ex} in figure 1, outside glial region G_3. The concentration in the synaptic cleft (at P_{syn}) reached steady state within 5 ms after release (Pendyam et al., 2009). The steady state extracellular concentration measured at P_{ex} was the same as at any other point outside the glial structures, i.e., negligible gradient outside the glial structures. Thus, steady state concentration at P_{syn} and P_{ex} were considered as output parameters for this study.

Iterative evaluation—Although the model applies to extracellular concentrations from the nM to mM range, we now consider a specific synapse that supports extracellular concentrations in the 4–5μM range. The iterative process for this synapse started with the glial configuration in figure 1 with parameter values in the lower end of the ranges as shown in table 1, while monitoring the concentrations of glutamate at P_{syn}, P_{mGluR}, and P_{ex} (figure 1) parameters were varied to determine values that satisfied model constraints. Based upon studies indicating that the highest densities of XAG were closer to the synapse (Cholet et al., 2002), G_1 had the highest surface density of XAG (see Table 1). The densities of XAG were varied in glial sheaths G, such that their relative proportions were maintained, i.e., density (G_1) > density (G_2) and so on. The equivalent surface density of XAG for configuration 1 (in figure 1) was determined iteratively by varying it within the range of 550–3,780 molecules/μm^2 (table 1). Due to the large surface area of the three sheath glial configuration considered, the density values considered were at the lower end of the experimentally reported range (2,500 – 10,000 molecules/μm^2; Bergles and Jahr, 1997; Lehre and Danbolt, 1998).

Experimental estimates of diffusion coefficients (D) in the perisynaptic region (i.e., < 1 μm from cleft) have not been reported for synapses with tightly packed glia. In the proposed model, with high density glia structures close to the synapse, we iteratively determined that diffusion coefficients in the range 0.05–0.1 μm^2/ms (table 1) satisfied model constraints. To compute the geometric tortuosity of configuration 1, we performed experiments with a point source as outlined in Tao and Nicholson, (2004). The estimated effective diffusion constant was approximately 10 times smaller than the microscopic D value. Similarly, iterative evaluation resulted in xc- production rate of 10 mM hr^{-1} (table 1) for configuration 1 to satisfy model constraints.

The glial geometry and parameter set derived represents one of the solutions that satisfied model constraints. Multiple solutions may exist based on glial geometry and parameter ranges. To study the role of glial configurations in neurotransmitter homeostasis, we used the present configuration as an example case.

Alternate model configurations

To study the effect of different glial geometries on neurotransmitter homeostasis for other ranges (nanomolar to micromolar range) of extracellular concentration, we considered multiple glial configurations (data not shown, also see Mohan et al. 2009). For example, we started with a porous glia geometry (similar to the perisynaptic model described model in Barbour, 2001; no glial sheaths), where we varied XAG numbers as part of parameter search to study the effect of transporter placement. This porous configuration was incapable of

supporting any neurotransmitter gradients due to homogenous distribution of transporters and the absence of impermeable glial structures around the cleft. To further probe the role of glial configurations (orientation, placement and number of folds) using impermeable sheaths, the following alternate geometries were considered: single sheath models with partial coverage (with 50%, 75% and 90%) ensheathment of synapse), two sheath models (with different orientations), and three sheath models (Mohan et al., 2009). The impermeable glial sheaths regulate the glutamate flux that lead to neurotransmitter gradients.

Synapses that support low extracellular concentrations (< 1 μM) required less than two sheaths, i.e., only partial coverage. But, for synapses supporting high extracellular concentrations (> 1 μM) configurations with multiple glial sheaths were required. Hence, we considered two and three sheath glial models to study their role in maintaining neurotransmitter gradients (configuration 1–3; see figures 1 and 2). Configuration 2 was similar to perisynaptic geometry described by Rusakov, (2001) and configuration 3 was a variation of configuration 2 with interleaved glial sheaths adding to the diffusion path length (defined as the distance that a molecule travels from the synaptic cleft to the extracellular space).

Model experiments showed that the parameters such as transporter density, diffusion, and xc-production played an important role in neurotransmitter homeostasis. For each configuration, a manual parameter search was conducted in the experimentally reported range for all parameters to determine parameter sets that satisfied all model constraints simultaneously. Furthermore, we developed a reduced order regression model for one of the configurations using the significant parameters to determine how these parameters affected the extracellular concentration.

RESULTS

As cited, an iterative process was employed to develop the model satisfying the constraints. We then used the model to obtain insights into the role of geometric and physiological parameters, such as the structure and number of glial sheaths, number of molecules per release, xc- production rate, diffusion coefficient, and XAG density, in establishing homeostasis in neurotransmitter concentrations. The methodology illustrated using the cortico-accumbens synapse is applicable to a general synapse that supports neurotransmitter gradients.

Steady state and transient characteristics

Using the iteratively determined model values listed in table 1, configuration 1 (figure 1) satisfied the cortico-accumbens model constraints, i.e., the steady state extracellular (at P_{ex}) and synaptic (at P_{syn}) glutamate concentrations at basal (2 Hz) and high frequency (15 Hz) presynaptic firing frequencies. Parameters that affected the steady state characteristics are discussed in detail in later sections.

Transient characteristics (measured for 200 ms after release) such as peak concentration and time course of neurotransmitter are critical for synaptic communication and prolonged presence of neurotransmitters in the cleft can cause excitotoxicity (Herman and Jahr, 2007).

The transient decay time course for neurotransmitter in the cleft is typically biphasic with initial peak amplitude of 1–4 μM, and with 100 us and 1–2 ms for the fast and slow time constants, respectively (Clements et al., 1992; Clements, 1996; Tong and Jahr, 1994). The model proposed in configuration 1 resulted in a peak synaptic concentration of 4 mM, with a biphasic profile and time constants of 120 μs and 2.1 ms, satisfying the transient characteristics. Perturbation studies (varying synaptic parameters by ± 10 and ± 20%) revealed that the peak amplitude of neurotransmitter concentration in the cleft depended on the number of molecules released and the size of the cleft. The decay time constants, however, were affected primarily by glial coverage, transporter density and diffusion coefficient while changes in extracellular neurotransmitter concentrations had no impact.

Influence of glial geometry—To study the influence of glial configurations on the extracellular neurotransmitter concentration, we considered configurations 2 and 3 (see figure 2; see 'Alternate model configurations' section in methods) by maintaining the same total number of transporter molecules as configuration 1. Configurations 2 and 3 did not satisfy model constraints (concentration gradients in the μM range) given the parametric values cited in table 1. For instance, to maintain extracellular concentrations in the 4–5 μM range as in configuration 1, the minimum synaptic concentration achievable for configuration 2 was seven-fold higher than the model constraint (i.e., 700 nM), and this can lead to excitotoxicity. Configuration 3 satisfied all constraints, but the parameter values (the number of transporters) exceeded physiological ranges by a factor of two. Thus, configuration 2 was not effective in maintaining synaptic concentration within physiological ranges for μM range concentrations at P_{ex}, as compared to configurations 1 and 3. This study highlights the role played by glial configurations in creating a diffusion path length, and providing 'isolation' (absent in configuration 2), for the class of synapses that support large (>1 μM) neurotransmitter gradients. However, it should be noted that synapses with lower extracellular neurotransmitter concentrations required far less glial coverage, as discussed later.

Sensitivity to model parameters

For configuration 1, each parameter was varied in the range ± 10–50% of their model values (table 1) to study the relative influence of the parameters on the concentrations at P_{syn}, P_{mGluR} and p_{ex}.

Transporter parameters

Total XAG molecules: Increasing the total XAG molecules in the range of 3,000 to 9,000 resulted in an exponential decrease in the extracellular and synaptic concentrations (figure 3a). For configuration 1, a 50% decrease/increase in total transporters caused a 33%/20% increase/decrease in concentration at P_{ex}. Synaptic steady state concentration reduced at a faster rate reaching half its maximum value with only a 15% increase in total transporters. This showed that variation in XAG had a much larger effect on the concentration at P_{syn} compared to that at P_{ex}. Increase in total transporter molecules increased uptake, as expected, decreasing concentrations at P_{ex} and P_{syn}.

XAG binding coefficients: The dissociation constant k_d (defined as k_{-1}/k_1) for transporters varies depending on the brain region (Lehre and Rusakov, 2002), and so the model was used to study the effect of varying XAG binding constants (i.e., k_{-1} and k_1). Although variation in XAG binding coefficients provided expected trends, the analysis quantified the effects. Increasing k_1 and k_2 independently by 50% resulted in the concentration at P_{ex} decreasing by 20% and 15%, respectively. With a 50% increase in k_{-1}, the concentration at P_{ex} increased by 16%. Further, with a 50%) decrease in k_1, k_2 and k_{-1}, the concentration at P_{ex} decreased by 30, 27, and −24 % (increase) respectively. These trends may be useful in evaluating the effects of these constants on synapses in other brain regions.

Non-synaptic neurotransmitter production—As cited, we considered the xc- production rate in the range 10–55 mM hr^{-1}. This resulted in a linear increase in both extracellular and synaptic concentrations, i.e., increase/decrease in xc-production by 50% from the operating point increased/decreased concentration at P_{ex} by 48% and 47%), respectively (figure 4a).

Diffusion coefficient—Increasing the diffusion coefficient in the range 0.025–0.075 $\mu m^2/ms$ resulted in an exponential decrease in extracellular concentration while the synaptic concentration increased linearly (figure 4b). A 50% increase/decrease in the diffusion coefficient from its operating point value decreased/increased concentration at P_{ex} by 18%/28% and increased/decreased concentration at P_{syn} by 30%/33%. Since diffusion controls the rate at which the molecules interact with XAG, concentration at P_{ex} increased as the extracellular molecules had difficulty entering the glial sheaths. Increasing the diffusion coefficient two-fold increased synaptic concentration by a factor of seven. Lowering diffusion values helped buffer molecules in the glial structures, facilitating their uptake and leading to a decreased concentration at the synapse.

Molecules per release and presynaptic firing frequency—No significant change in extracellular concentration was observed when presynaptic firing frequencies and number of molecules per release were varied ± 50% around the model values. Varying the number of molecules per release in the range 2,000–20,000 resulted in no change in the concentration at P_{syn} and P_{ex}, for the basal 2 Hz case (figure 4c), indicating rapid clearance by the transporters. As cited, firing frequencies of cortico-accumbens synapses vary from 1–15 Hz (Sun and Rebec, 2006). At the lower range of these frequencies (< 8 Hz), varying the number of molecules per release had no significant impact on the concentration at P_{ex}. At higher frequencies (>10 Hz), an increase of about 10% was observed at P_{ex} and a two-fold increase was observed at p_{syn}.

In summary, the findings from the parametric studies were that the glial configuration had the greatest impact on neurotransmitter homeostasis, followed by, in order, non-synaptic sources, transporter densities/binding constants, and diffusion coefficient. These insights have been used to provide guidelines for reverse engineering general synapses, as described later.

Direction of flux reveals influence of non-synaptic sources on mGluR receptors

In order to study the influence of synaptic and nonsynaptic sources on autoreceptor activation we monitored the flux flow at the edge of the glia G_3 in figure 1. Synaptic release caused a sudden outward flux at this surface towards the extracellular space. After this transient event, there is a steady lower magnitude flux (driven by non-synaptic sources, see figure 5) towards the synapse which lasts till the subsequent release. Varying release properties i.e., increasing the the number of molecules per release or firing rate delayed the switch in flux direction, neurotransmitter were directed towards extracellular space for longer duration. Varying diffusion coefficient, xc- production and transporter parameters changed the magnitude of flux flow without much change in duration of flux direction. In all sensitivity studies (see above) we found that the flux flow after release was transient and outwards (away from synapse) while reminder of the time before next release event, steady flow of inwards flux towards synapse was observed. This flux was due to non-synaptic sources which effect the autoreceptor activation. To further check the tone on autoreceptors, we inactivated the synaptic release and found a steady flow of flux towards the synapse caused due to non-synaptic sources. The model experiments predicted that steady, persistent flow of flux towards synapse for long periods of time after release are responsible for the tone on mGlur2/3 autoreceptors compared to transient synaptic release.

The model also shows that the magnitude of this steady state inward flux can quantify the synaptic isolation provided by glial structure and perisynaptic parameters. To study this we measure the flux flow at the opening of glial sheath G_1 (see figures 1 and 2; between shell i=2 and 3 and radial compartment j=1). The average steady state flux values for configurations 1, 2, and 3 were in the ratio 10:1:6, showing the isolation provided by each configuration.

DISCUSSION

The computational models provided several insights for general synapses that support gradients in neurotransmitter concentrations between the cleft and the extracellular space. Although configuration 1 was utilized for several of the studies, the trends are expected to be similar for other configurations also.

Models experiments predict that effective synaptic isolation for synapses with > 1 μM extracellular concentrations requires specific glial configurations

It was seen that a configuration with permeable glia could not support neurotransmitter gradients and resulted in a uniform concentration profile throughout the perisynaptic space. We also observed, permeable glia and configurations 2 and 3 resulted in very different neurotransmitter concentration values with the same set of parameters, highlighting the role of glial configuration. Further, configurations 2 and 3 had lower uptake numbers? compared to the permeable glial configuration, highlights the role of transporter placement on glial folds, we propose that placement of glutamate transporter proteins modulates extracellular concentration via its interaction with diffusing neurotransmitters. Also, an appropriate diffusion coefficient constrained the influx of the neurotransmitter molecules from the

extracellular space through the glial sheaths. All this collectively helped achieve synaptic 'isolation' to maintain concentrations gradients.

The simulated model provided an effective tool to characterize/quantify the interplay between glial configuration, glutamate transporter protein placement and tortuosity, in generating the required diffusion path length for synaptic isolation and sustenance of neurotransmitter gradients. figure 6 illustrates correlation between three parameters, namely, transporter density, xc- production rate, and diffusion coefficient, (all satisfying synaptic constraints) to maintain a specific concentration at P_{ex}, for the cortico-accumbens synapse in configuration 1. This characterization further implied that glial configurations for synapses with < 1 μM extracellular concentrations have simpler geometric structures and would require comparatively less transporter molecules, and lower or zero non-synaptic production rates.

Simulated model demonstrated that to maintain an extracellular concentration > 1 μM the glial configuration should provide longer diffusion path length to increases the time neurotransmitter molecules spends in glial environment. A reduced diffusion coefficient and increased transporter binding rates can result in the similar effect. However, simulated model experiments showed that reducing diffusion coefficient or increasing transporter binding constants in physiological parameter ranges was not sufficient to maintain high (> 1 μM) extracellular neurotransmitter concentrations. Hence, for synapses that maintain concentration gradient in the range > 1 μM require complicated glial configuration.

Non-synaptic sources are required to maintain μM level extracellular concentrations

To study the contribution of synaptic and non-synaptic sources in maintaining extracellular glutamate concentrations, we varied the number of molecules per release within physiological ranges of 2,000–20,000 with no non-synaptic sources, for configuration 1, at a basal firing rate of 2 Hz. The transporters located on the glial sheath G_1 ensured rapid elimination of neurotransmitters even with large number of molecules per release, indicating little impact of molecules/release on extracellular concentration. At higher presynaptic firing rates (> 10 Hz) that have been reported during bursts (Sun and Rebec, 2006), a modest increase of 10% was observed at P_{ex}. Thus, neurotransmitter release primarily activates postsynaptic receptors and does not contribute significantly to the extracellular concentration for such synapses.

This, in turn, implies that non-synaptic glutamate sources help maintain extracellular concentrations An increase/decrease in non-synaptic production rate in the absence of synaptic release resulted in a proportional increase/decrease in the extracellular concentration. In the simulated model, non-synaptic sources along with glial sheaths help establish and maintain gradients. Our results are in agreement with recent microdialysis studies (Melendez et al., 2005) and cell culture/tissue slice experiments (Jabaudon et al., 1999; Haydon, 2001) which report that glutamate outside of the cleft is not of synaptic origin.

Transporter and non-synaptic source densities can co-vary to provide tone on presynaptic autoreceptors

The model experiments predicted that under homeostatic conditions, the tone on the presynaptic autoreceptors (mGluR2/3; measured as concentration at P_{mGluR}) was provided by extracellular neurotransmitter, i.e., there was a constant influx of molecules that established a baseline tone (50%) on the autoreceptor in configuration 1. This prediction was in agreement with experimental reports (Xi et al., 2002; Moran et al., 2005) that show tone on mGluR2/3 (at P_{mGluR} in figure 1) being derived primarily from non-synaptic sources and stimulating these receptors would affect the synaptic release.

The simulated model also revealed the ratio of xc- production rate to XAG density had to be constant to maintain the same baseline tone on mGluR. During pathological or physiological conditions, dysregulation of one of the mechanisms, e.g., xc- or XAG, could be compensated by the other mechanisms to maintain tone. This prediction was recently validated in cocaine affected cortico-accumbens synapses where the glutamate transporter GLT-1 were down regulated (Kalivas, 2009; Knackstedt et al., 2010) to compensate for decrease in xc- production previously reported for these synapses (Baker et al., 2003).

Model experiments suggest a correlation between transporters and xc- production, and that synapses with smaller gradients require less glial coverage and fewer transporters. To avoid excitotoxic damage, this would also suggest that these same regions might have markedly lower levels of xc- density. Support for this comes from a comparison of reported extracellular concentration (glutamate), glial coverage and xc- density levels for synapses from five different brain regions: hippocampus (mossy fiber-CA3), cerebellum (climbing fiber-Purkinje cell), cortex (input synapses to layer 5 pyramidal cells), striatum and nucleus accubens. Specifically, extracellular glutamate concentrations for these synapses were as follows: 25nM for hippocampus (Herman and Jahr, 2007), 600 nM for cerebellum (Mark et al., 2001), 1.2 μM for cortex (Baker, 2003), 2.4 μM for striatum (Baker, 2003), and 5.6 μM for accumbens (Baker, 2003). These concentrations were highly correlated to the glial coverage: synapses in hippocampus had no significant glial coverage (Rollenhagen and Lubke, 2006), only 50% of cerebellar synapses had about 90% coverage (Xu-Friedman et al., 2001), while cortical synapses were completely covered with glial processes (Rollenhagen and Lubke, 2006), and dense glial coverage was observed in the striatum (Villalba and Smith, 2011). Our previous study suggested that accumbal synapses are densely ensheathed by glia (Pendyam et al., 2009).

Also, a correlation was seen between xc- exchanger density and extracellular concentration levels for different synapse types. The density of xc- exchangers in the cortex is 2.4-fold higher than in the cerebellum (Warr et al., 1999). This provides validation for the model prediction that extracellular concentration is correlated to glial coverage, and to the density of transporters and xc-.”

Synaptic glial configuration can be proposed for a given extracellular concentration

We used the example case cortico-accumbens synapse to illustrate how the reverse engineering insights related to glial coverage, transporter placement and diffusion

coefficient be used to propose probable synaptic glial configurations, for a specified extracellular concentration. It should be noted that other glial geometries that provide the same resistance to flow would also be feasible candidates.

Proposed configurations for concentrations < 1 μM at P_{ex}—For synapses with extracellular concentration values (at P_{ex}) less than 1 μM, all three proposed configurations (see figures 1 and 2) were feasible. That is, they satisfied the transmitter decay profile, steady state synaptic concentration to avoid receptor excitotoxicity (< 100 nM), and supported extracellular concentrations within the 1 μM range for high presynaptic frequencies. Configurations 1 and 3 achieved concentration levels less than 1 μM with lower transporter densities (< 2,500 molecules/μm^2; other predicted parameters in table 2) compared to configuration 2 which required transporter densities in a range of 2,500–5,000 molecules/μm^2. It should be noted that in addition to configuration 1–3, other configurations such as a one sheath glial model with partial coverage (with 50%, 75% and 90% ensheathment of synapse) satisfied model constraints for neurotransmitter concentration in the range < *1 μM*.

Proposed configurations for concentrations of 1 μM −5 μM at P_{ex}—Configurations 1 and 3 achieved extracellular concentrations in the range of 1–5 μM and simultaneously satisfied model constraints. Configuration 3 required more than two-fold increases in transporter density (4,500–7,500 molecules/μm^2) and xc- production rates (40–65 mM hr^{-1}; other predicted parameters in table 3), compared to its < 1 μM case. Configuration 1 required transporter density of 1,500–4,500 molecules/μm^2 and xc- production rates in the range 10–40 mM hr^{-1} to maintain extracellular concentration in the range 1–5 μM at P_{ex}. As cited, configuration 2 could not maintain extracellular concentrations > 1 μM with P_{syn} within the 100–200 nM range, and with parameters within physiological ranges.

Proposed configurations for concentrations of > 5 μM at P_{ex}—For extracellular concentrations greater than 5 μM, configuration 1 with three glial sheaths satisfied all model constrains. When compared to the 1 μM −5 μM case, this required a two-fold increase in both the transporter density (3,000–10,500 molecules/μm^2), and xc- production rate (40–75 mM hr^{-1}; other predicted parameters in table 2). So, for synapses with large neurotransmitter gradients, the glial coverage is predicted to be very tight.

In summary, the proposed model provides guidelines for the selection of glial configurations and parameter values (e.g., transporters, non-synaptic sources, and diffusion coefficient, as in figure 6) for general synapses supporting gradients.

Reduced order model to predict extracellular concentration

The sensitivity analysis revealed that xc- production, transporter density and diffusion coefficient were the key parameters to predict extracellular concentration for configuration 1, which has the synaptic ‘isolation’ necessary to maintain extracellular concentrations in the micromolar range. Such a reduced order model was developed based on estimates from configuration 1. Initially we held xc- production constant at 100 molecules/ms (or 9.96 mM

hr^{-1}) and varied both transporter density and diffusion coefficients in the range reported in table 1 and determined the corresponding extracellular concentration levels. To relate the two parameters to extracellular concentration (for a fixed xc- rate), we found the reduced order model shown in equation 4,

$$\text{Extracellular concentration} = a \times T^b \times D^c \quad (4)$$

In eqn. 4, T is transporter density (molecules/μm^2) and D is diffusion coefficient (μm/ms). Now varying the third parameter, xc- productions rate, we found the relationship between the coefficients a, b, and c in eqn. 4 and xc^- production rate (mM hr^{-1}). For configuration 1, coefficient 'a' was of a polynomial form $a=\sum_{i=0}^{2} P_i (xc-)^{2i} + \sum_{i=1}^{3} q_i (xc-)^{-2i}$ with P_i = {6.02×10^{-4}, 5.32×10^{-5}, 5.71×10^{-8}} and q_i = {0.0351,−0.746, 3.35}, and coefficients 'b' and 'c' were of the form $b=\sum_{i=1}^{5} b_i (xc-)^i$ and $c=\sum_{i=1}^{5} c_i (xc-)^i$ with b_i = {−0.893, 0.0184, -4.48×10^{-3}, 3.47×10^{-4}, -1.28×10^{-5}, 1.71×10^{-7}} and c_i = {−0.129, −0.0241, 3.43×10^{-3}, -3.07×10^{-4}, 1.39×10^{-5}, -2.56×10^{-7}}, respectively. In addition to the finding that extracellular concentration could be completely characterized by xc- production rate, transporter density and diffusion coefficient, the reduced order model reveals that uptake rate also depends on xc- production.

The model in configuration 1 can used to achieve extracellular concentrations within the range 0.7–15 μM by varying xc- production, transporter density and diffusion coefficient within their own specific ranges, via a relationship described in equation 4.

Limitations and future work

Glial configurations very close to synapses are not well understood, particularly for synapses that support gradients between the cleft and the extracellular space. Accordingly, the configurations proposed should be viewed as being only *equivalent* in that they provide the same resistance to the flow of neurotransmitter such as spines, small axonal boutons and microglia. Refined experimental estimates for the ranges of many of the parameters (table 1) would enhance model predictions. In particular, diffusion coefficients close to the synapse have not been reported and model predictions show that they have to be somewhat low for homeostasis under the conditions considered. It is also noted that the xc- exchanger model had a constant glutamate release. In reality, increase in extracellular concentration would inhibit the influx of cystine by "homo-exchange" with glutamate, reducing the production of glutamate (Warr et al., 1999). In model experiments, the steady state extracellular concentration variations with such a variable release were within 10–20%, and so we assumed a constant efficiency for the xc- exchanger. Future models could include a kinetic scheme for xc- exchange with dependence on both glutamate and cystine concentrations. As cited earlier, there is lack of consensus on the range of extracellular neurotransmitter concentrations *in vivo* due to the different types of estimation methods used. However, the proposed model is independent of the extracellular concentration levels, and provides a framework to study the mechanisms required for maintaining homeostasis for a wide range

of extracellular concentrations, from nanomolar to micromolar levels. On-going studies are focused on gaining additional insights using Monte Carlo approaches with stochastic molecular dynamics and boulder-like glial structures and to develop multiple synapse models to study cross-talk between synapses.

CONCLUSION

A computational framework was proposed to reverse engineer glial configuration and parameters for a class of synapses that support neurotransmitter gradients between the cleft and the extracellular space. The models provided several insights and predictions pertaining to the role of glial configuration in isolating the synapse, and to the relative importance of parameters such as glial configuration, diffusion coefficient, transporter density and distribution, molecules per release and non-synaptic production, on neurotransmitter homeostasis. Consistent with experimental reports, the model predicted that non-synaptic sources are necessary for both neurotransmitter homeostasis, and for maintaining tone on the presynaptic autoreceptors, for the example case. The proposed computational models and the trends they predicted are applicable to general synapses that support gradients.

ACKNOWLEDGEMENTS

We thank the United States Public Health Service for grants supporting this work.

REFERENCES

Alagarsamy S, Sorensen SD, Conn PJ. Coordinate regulation of metabotropic glutamate receptors. Curr Opin Neurobiol. 2001; 11:357–362. [PubMed: 11399435]

Baker DA, McFarland K, Lake RW, Shen H, Tang XC, Toda S, Kalivas PW. Neuroadaptations in cystine-glutamate exchange underlie cocaine relapse. Nature Neurosci. 2003; 6:743–749. [PubMed: 12778052]

Barbour B. An evaluation of synapse independence. J Neurosci. 2001; 21:7969–7984. [PubMed: 11588170]

Bergles DE, Jahr CE. Synaptic activation of glutamate transporters in hippocampal astrocytes. Neuron. 1997; 19:1297–1308. [PubMed: 9427252]

Bergles DE, Jahr CE. Glial contribution to glutamate uptake at schaffer collateral-commissural synapses in hippocampus. J Neurosci. 1998; 18:7709–7716. [PubMed: 9742141]

Billups B, Graham BP, Wong AY, Forsythe ID. Unmasking group III metabotropic glutamate autoreceptor function at excitatory synapses in the rat CNS. J Physiol. 2005; 565:885–896. [PubMed: 15845577]

Bouvier M, Szatkowski M, Amato A, Attwell D. The glial cell glutamate uptake carrier counter transports pH-changing anions. Nature. 1992; 360:471–474. [PubMed: 1448171]

Bridges RJ. System xc- cystine/glutamate antiporter: An update on molecular pharmacology and roles within the CNS. Br J Pharmacol. 2011

Bruns D, Jahn R. Real-time measurement of transmitter release from single synaptic vesicles. Nature. 1995; 377:62–65. [PubMed: 7659162]

Chang JY, Zhang L, Janak PH, Woodward DJ. Neuronal responses in prefrontal cortex and nucleus accumbens during heroin self-administration in freely moving rats. Brain Res. 1997; 754:12–20. [PubMed: 9134954]

Cholet N, Pellerin L, Magistretti PJ, Hamel E. Similar perisynaptic glial localization for Na+, K+-ATPase alpha 2 subunit and the glutamate transporters GLAST and GLT-1 in the somatosensory cortex. Cerebral Cortex. 2002; 12:515–525. [PubMed: 11950769]

Clements JD. Transmitter time course in the synaptic cleft: its role in central synaptic function. Trends Neurosci. 1996; 19:163–171. [PubMed: 8723198]

Clements JD, Robin A, Lester J, Tong G, Jahr CE, Westbrook GL. The time course of glutamate in the synaptic cleft. Science. 1992; 258:1498–1501. [PubMed: 1359647]

Danbolt NC. Glutamate uptake. Prog Neurobiol. 2001; 65:1–105. [PubMed: 11369436]

Day BK, Pomerleau F, Burmeister JJ, Huettl P, Gerhardt GA. Microelectrode array studies of basal and Potassium-evoked release of L-glutamate in the anesthetized rat brain. J Neurochem. 2006; 96:1626–1635. [PubMed: 16441510]

Diamond JS. Deriving the glutamate clearance time course from transporter currents in CA1 hippocampal astrocytes: transmitter uptake gets faster during development. J Neurosci. 2005; 25:2906–2916. [PubMed: 15772350]

Diamond JS, Jahr CE. Transporters buffer synaptically released glutamate on a sub millisecond time scale. J Neurosci. 1997; 17:4672–4687. [PubMed: 9169528]

Dietrich D, Kral T, Clusmann H, Friedl M, Schramm J. Presynaptic group II metabotropic glutamate receptors reduce stimulated and spontaneous transmitter release in human dentate gyrus. Neuropharmacology. 2002; 42:297–305. [PubMed: 11897108]

Ding J, Peterson JD, Surmeier DJ. Corticostriatal and thalamostriatal synapses have distinctive properties. J Neurosci. 2008; 28:6483–6492. [PubMed: 18562619]

Featherstone DE, Shippy SA. Regulation of synaptic transmission by ambient extracellular glutamate. The Neuroscientist. 2008; 14:171–181. [PubMed: 17947494]

Franks KM, Bartol TM, Sejnowski TJ. A Monte Carlo model reveals independent signaling at central glutamatergic synapses. Biophys J. 2002; 83:2333–2348. [PubMed: 12414671]

Haydon P. Glia: listening and talking to the synapse. Nature Neurosci. 2001; 2:185–191.

Herman MA, Jahr CE. Extracellular glutamate concentration in hippocampal slice. J Neurosci. 2007; 27:9736–9741. [PubMed: 17804634]

Jabaudon D, Shimamoto K, Yasuda-Kamatani Y, Scanziani M, Gahwiler BH, Gerber U. Inhibition of uptake unmasks rapid extracellular turnover of glutamate of nonvesicular origin. PNAS. 1999; 96:8733–8738. [PubMed: 10411944]

Kalivas PW. The glutamate homeostasis hypothesis of addiction. Nature Rev Neurosci. 2009; 10:561–572. [PubMed: 19571793]

Knackstedt LA, LaRowe S, Mardikian P, Malcolm R, Upadhyaya H, Hedden S, Markou A, Kalivas PW. The role of cystine-glutamate exchange in nicotine dependence in rats and humans. Biol Psychiatry. 2009; 65:841–845. [PubMed: 19103434]

Knackstedt LA, Melendez IR, Kalivas PW. Ceftriaxone restores glutamate homeostasis and prevents relapse to cocaine seeking. Biol Psychiatry. 2010; 67:81–84. [PubMed: 19717140]

Lehre KP, Danbolt NC. The number of glutamate transporter subtype molecules at glutamatergic synapses: chemical and stereological quantification in young adult rat brain. J Neurosci. 1998; 18:8751–8757. [PubMed: 9786982]

Lehre KP, Rusakov D. Asymmetry of glia near synapse favors presynaptic glutamate escape. Biophys J. 2002; 83:125–134. [PubMed: 12080105]

Losonczy A, Somogyi P, Nusser Z. Reduction of excitatory postsynaptic responses by persistently active metabotropic glutamate receptors in the hippocampus. J Neurophysiol. 2003; 89:1910–1919. [PubMed: 12686572]

LoTurco JJ, Owens DF, Heath MJ, Davis MB, Kriegstein AR. GABA and glutamate depolarize cortical progenitor cells and inhibit DNA synthesis. Neuron. 1995; 15:1287–1298. [PubMed: 8845153]

Manent JB, Represa A. Neurotransmitters and brain maturation: early paracrine actions of GABA and glutamate modulate neuronal migration. The Neuroscientist. 2007; 13:268–279. [PubMed: 17519369]

Mark LP, Prost RW, Ulmer JL, Smith MM, Daniels DL, Strottmann JM, Brown WD, Hacein-Bey L. Pictorial review of glutamate excitotoxicity: fundamental concepts for neuroimaging. Am J Neuroradiol. 2001; 22:1813–1824. [PubMed: 11733308]

Melendez RI, Vuthiganon J, Kalivas PW. Regulation of extracellular glutamate in the prefrontal cortex: focus on the cystine glutamate exchanger and group I metabotropic glutamate receptors. J Pharmacol Exp Ther. 2005; 314:139–147. [PubMed: 15769865]

Mohan A, Pendyam A, Kalivas PW, Nair SS. Molecular diffusion model of neurotransmitter homeostasis around synapses supporting gradients. Neural Comput. 2010; 23:984–1014. [PubMed: 21222526]

Moran MM, McFarland K, Melendez RI, Kalivas PW, Seamans JK. Cystine/glutamate exchange regulates metabotropic glutamate receptor presynaptic inhibition of excitatory transmission and vulnerability to cocaine seeking. J Neurosci. 2005; 25:6389–6393. [PubMed: 16000629]

Moussawi K, Riegel A, Nair S, Kalivas PW. Extracellular glutamate: functional compartments operate in different concentration ranges. Front Syst Neurosci. 2011; 5:94. [PubMed: 22275885]

Murthy VN, Sejnowski TJ. Heterogeneous release properties of visualized individual hippocampal synapses. Neuron. 1997; 18:599–612. [PubMed: 9136769]

Nicholson C, Sykova E. Extracellular space structure revealed by diffusion analysis. Trends Neurosci. 1998; 21:207–215. [PubMed: 9610885]

Nicholson C. Diffusion and related transport mechanism in brain tissue. Rep Prog Phys. 2001; 64:815–884.

Nguyen L, Rigo JM, Rocher V, Belachew S, Malgrange B, Rogister B, Leprince P, Moonen G. Neurotransmitters as early signals for central nervous system development. Cell Tissue Res. 2001; 305:187–202. [PubMed: 11545256]

Nyitrai G, Kekesi KA, Juhasz G. Extracellular level of GABA and Glu: in vivo microdialysis-HPLC measurements. Curr Top Med Chem. 2006; 6:935–940. [PubMed: 16787267]

Patneau DK, Mayer ML. Structure-activity relationships for amino acid transmitter candidates acting at N-methyl-D-aspartate and quisqualate receptors. J Neurosci. 1990; 10:2385–2399. [PubMed: 2165523]

Pendyam S, Mohan A, Kalivas PW, Nair SS. Computational model of extracellular glutamate in the nucleus accumbens incorporates the impact by chronic cocaine. Neuroscience. 2009; 158:1266–1276. [PubMed: 19084053]

Peters YM, O'Donnell P, Carelli RM. Prefrontal cortical cell firing during maintenance, extinction, and reinstatement of goal-directed behavior for natural reward. Synapse. 2005; 56:74–83. [PubMed: 15729742]

Reissner KJ, Kalivas PW. Using glutamate homeostasis as a target for treating addictive disorders. Behav Pharmacol. 2010; 21:514–22. [PubMed: 20634691]

Rollenhagen A, Lubke JHR. The morphology of excitatory central synapses: from structure to function. Cell Tissue Res. 2006; 326:221–237. [PubMed: 16932936]

Rusakov DA. The role of perisynaptic glial sheaths in glutamate spillover and extracellular Ca2+ depletion. Biophys J. 2001; 81:1947–1959. [PubMed: 11566769]

Rusakov DA, Kullmann DM. Extrasynaptic glutamate diffusion in the hippocampus: ultrastructural constraints, uptake, and receptor activation. J Neurosci. 1998; 18:3158–3170. [PubMed: 9547224]

Saftenku EE. Modeling of slow glutamate diffusion and AMPA receptor activation in the cerebellar glomerulus. J Theor Biol. 2005; 234:363–382. [PubMed: 15784271]

Sato H, Tamba M, Okuno S, Sato K, Keino-Masu K, Masu M, Bannai S. Distribution of cystine/glutamate exchange transporter, system x(c)-, in the mouse brain. J Neurosci. 2002; 22:8028–8033. [PubMed: 12223556]

Schoepp DD, True RA. 1S-3R-ACPD-sensitive (metabotropic) [3H] glutamate receptor binding in membranes. Neurosci Lett. 1992; 145:100–104. [PubMed: 1461560]

Squire, LR.; Roberts, JL.; Spitzer, NC.; Zigmond, MJ. Fundamental Neuroscience. Third Edition.. Elsevier Science & Technology Books; 2002.

Sun W, Rebec GV. Repeated cocaine self-administration alters processing of cocaine-related information in rat prefrontal cortex. J Neurosci. 2006; 26:8004–8008. [PubMed: 16870745]

Sykova E. Extrasynaptic volume transmission and diffusion parameters of the extracellular space. Neuroscience. 2004; 129:861–876. [PubMed: 15561404]

Tanaka K, Watase K, Manabe T, Yamada K, Watanabe M, Takahashi K, Iwama H, Nishikawa T, Ichihara N, Kikuchi T, Okuyama S, Kawashima N, Hori S, Takimoto M, Wada K. Epilepsy and exacerbation of brain injury in mice lacking the glutamate transporter GLT-1. Science. 1997; 276:1699–1702. [PubMed: 9180080]

Tao L, Nicholson C. Maximal geometrical hindrance to diffusion in brain ECS surrounding uniformly spaced convex cells. J Theor Biol. 2004; 229:59–68. [PubMed: 15178185]

Tao A, Tao L, Nicholson C. Cell cavities increase tortuosity in brain extracellular space. J Theor Biol. 2005; 234:525–536. [PubMed: 15808873]

Thorne RG, Nicholson C. In vivo diffusion analysis with quantum dots and dextrans predicts the width of brain extracellular space. PNAS. 2006; 103:5567–72. [PubMed: 16567637]

Tong G, Jahr CE. Block of glutamate transporters potentiates postsynaptic excitation. Neuron. 1994; 13:1195–1203. [PubMed: 7946356]

Trantham H, Szumlinski K, McFarland K, Kalivas PW, Lavin A. Repeated cocaine administration alters the electrophysiological properties of prefrontal cortical neurons. Neuroscience. 2002; 113:749–757. [PubMed: 12182882]

Trommershauser J, Schneggenburger R, Zippelius A, Neher E. Heterogeneous presynaptic release probabilities: functional relevance for short-term plasticity. Biophys J. 2003; 84:1563–1569. [PubMed: 12609861]

van der Zeyden M, Oldenziel WH, Rea K, Cremers TI, Westerink BH. Microdialysis of GABA and glutamate: Analysis, interpretation and comparison with microsensors. Pharmacol Biochem Behav. 2008; 90:135–147. [PubMed: 17939932]

Villalba RM, Smith Y. Front Neuroglial plasticity at striatal glutamatergic synapses in Parkinson's disease. Syst Neuro sci. 2011; 5:68.

Warr O, Takahashi M, Attwell D. Modulation of extracellular glutamate concentration in rat brain slices by cystine-glutamate exchange. J Physiol. 1999; 514:789–793.

Wolf ME. The Bermuda Triangle of cocaine-induced neuroadaptations. Trends Neurosci. 2010; 33:391–388. [PubMed: 20655604]

Wyatt I, Gyte A, Simpson MG, Widdowson PS, Lock EA. The role of glutathione in L-2-chloropropionic acid induced cerebellar granule cell necrosis in the rat. Arch Toxicol. 1996; 70:724–735. [PubMed: 8896718]

Xi ZX, Baker DA, Shen H, Carson DS, Kalivas PW. Group II metabotropic glutamate receptors modulate extracellular glutamate in the nucleus accumbens. J Pharmacol Exp Ther. 2002; 300:162–171. [PubMed: 11752112]

Xu-Friedman MA, Harris KM, Regehr WG. Three-dimensional comparison of ultrastructural characteristics at depressing and facilitating synapses onto cerebellar Purkinje cells. J Neurosci. 2001; 21:6666–6667. [PubMed: 11517256]

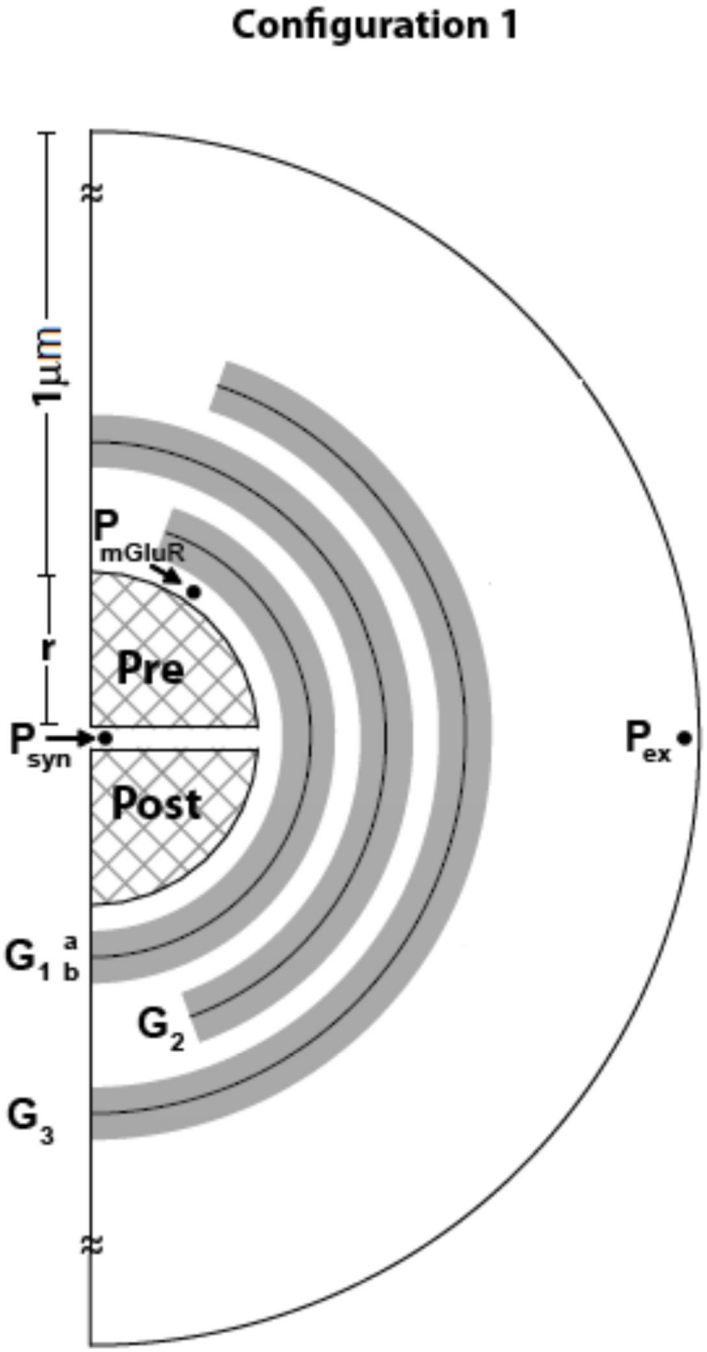

Figure 1.

Schematic of configuration 1, with transporters and non-synaptic sources in glial regions *(shaded)*. The cleft (δ =20 nm) separates the two hemispheres of radii *r* = 160 nm, surrounded by glial sheaths (G_i, *i*=1–3; *i*=1 being the closest to the synapse) with the highest density of transporters in G_1 and decreasing in radially outward sheaths. Each sheath was 50 nm thick with an impermeable surface in the middle, and with transporters volume populated in the 25 nm thick space on either side, permitting interaction with neurotransmitter molecules. xc- was volume populated only on sheath G_{3b} The perisynaptic

space was partitioned in radial (step σ =25 nm) and tangential (step θ =20°) directions as in Rusakov, (2001) with the dimension of the opening being 20° from the vertical. Binding, uptake and efflux are computed for each compartment. Neurotransmitter concentrations were measured at three sites, within the synaptic cleft (at P_{syn}), in the perisynaptic region containing presynaptic mGluR (at P_{mGluR}), and at the site of a dialysis probe (at P_{ex}).

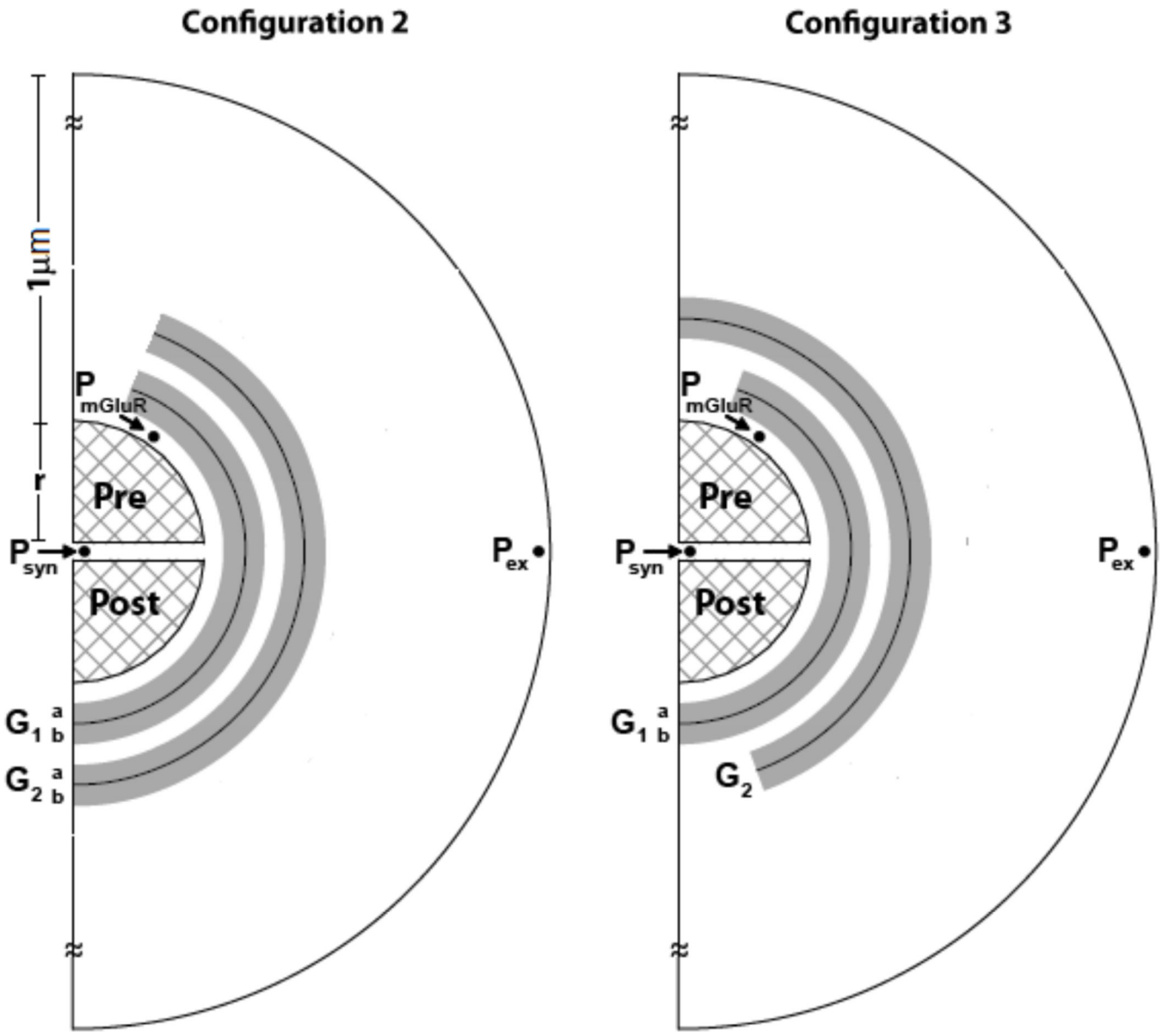

Figure 2.

Two additional glial configurations used to study neurotransmitter homeostasis in the perisynaptic space (see figure 1 for locations where measurements are made). **A. configuration 2:** The presynaptic opening reduces the diffusion path length. **B. configuration 3:** Intermediate configuration that adds more diffusion path length compared to configuration 2, but not as much as in configuration 1.

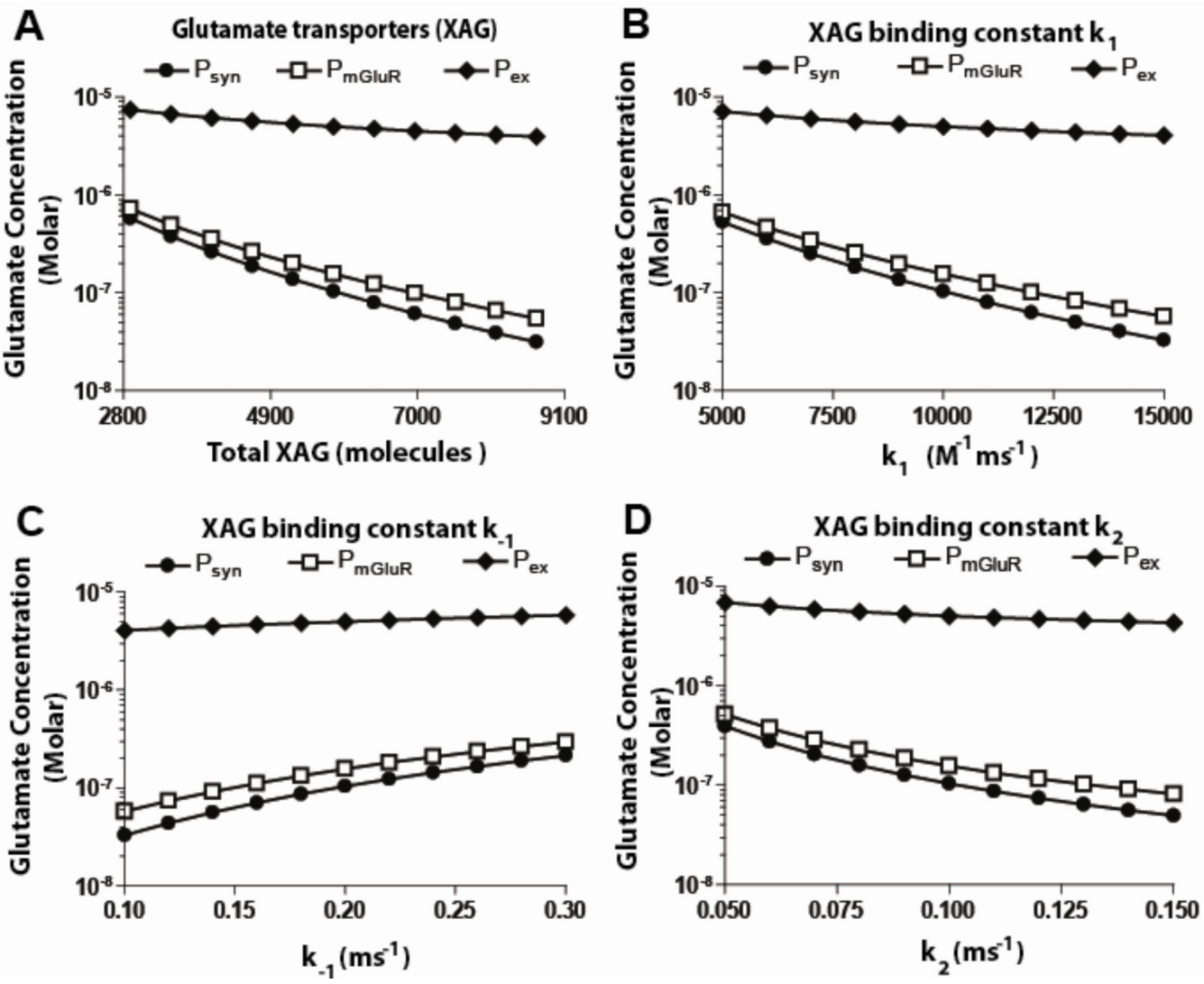

Figure 3.

Effect of varying transporter parameters (others model values from table 1) on glutamate concentrations at three spatial locations under basal conditions, for configuration 1. **A**. An increase in transporters resulted in a significant drop in concentrations at P_{syn} and P_{mGluR}, but only a minor drop at P_{ex}. **B**. As the forward binding constant (k_1) was increased, the concentration of glutamate decreased at P_{syn} and $P_{mGluR,}$ with little change at P_{ex}. **C**. As the reverse binding constant (k_{-1}) was increased, concentrations at P_{syn} and P_{mGluR} increased, while concentration at P_{ex} remained constant. **D**. As the binding constant (k_2) was increased, concentration at P_{syn} and P_{mGluR} decreased while it was constant at P_{ex} (see figure 1 for locations where measurements are made).

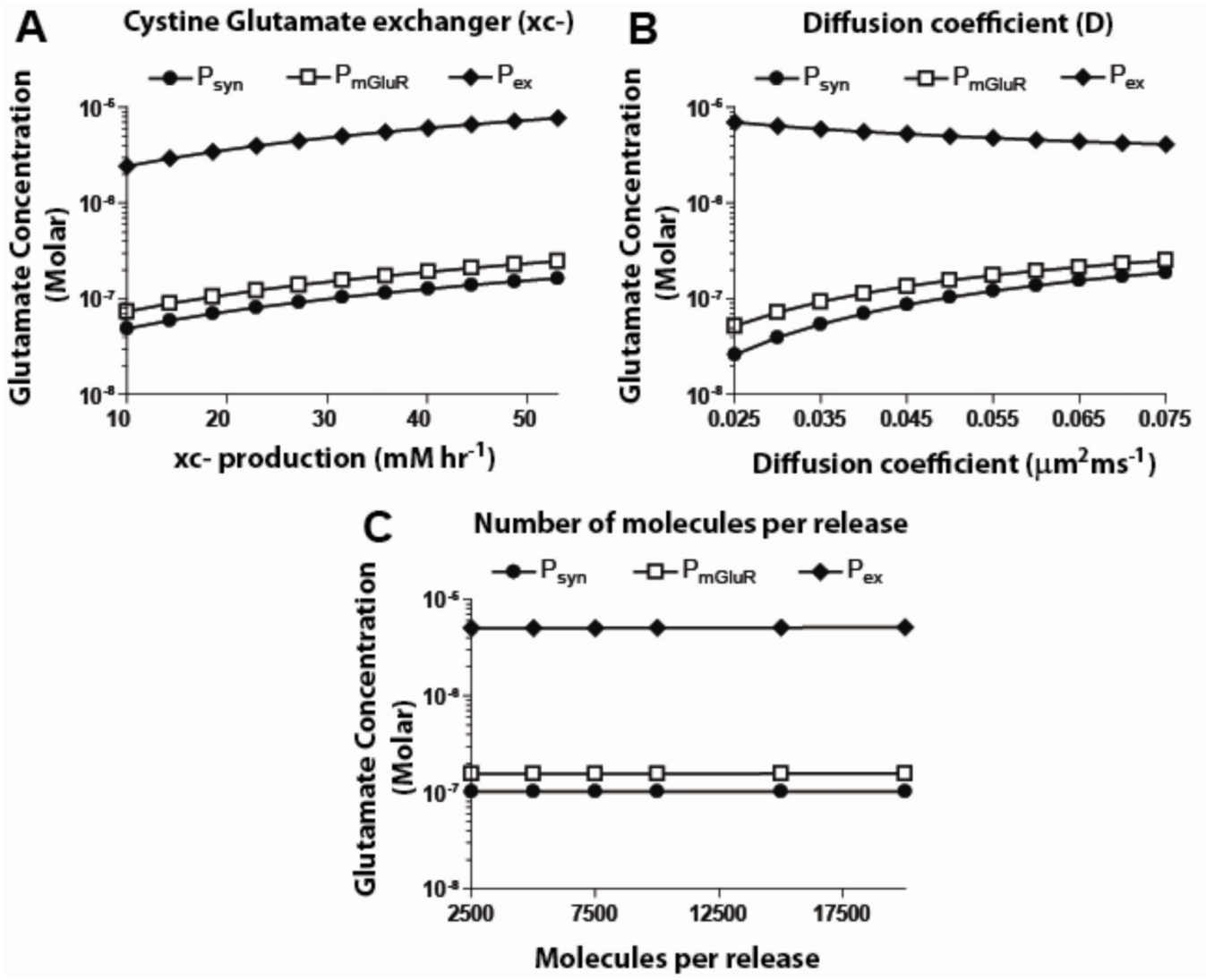

Figure 4.

Effect of varying other parameters (rest of the model values from table 1) on glutamate concentrations at three spatial locations under basal conditions, for configuration 1. **A**. An increase in xc- production rate resulted in increased concentrations at $P_{syn,}$ P_{mGluR} and P_{ex}. **B**. Increasing diffusion coefficient values resulted in increased glutamate concentrations at P_{syn} and $P_{mGluR,}$ but decreased values at P_{ex}. **C**. Altering the molecules per release resulted in no change in the concentrations at any location (see figure 1 for locations where measurements are made).

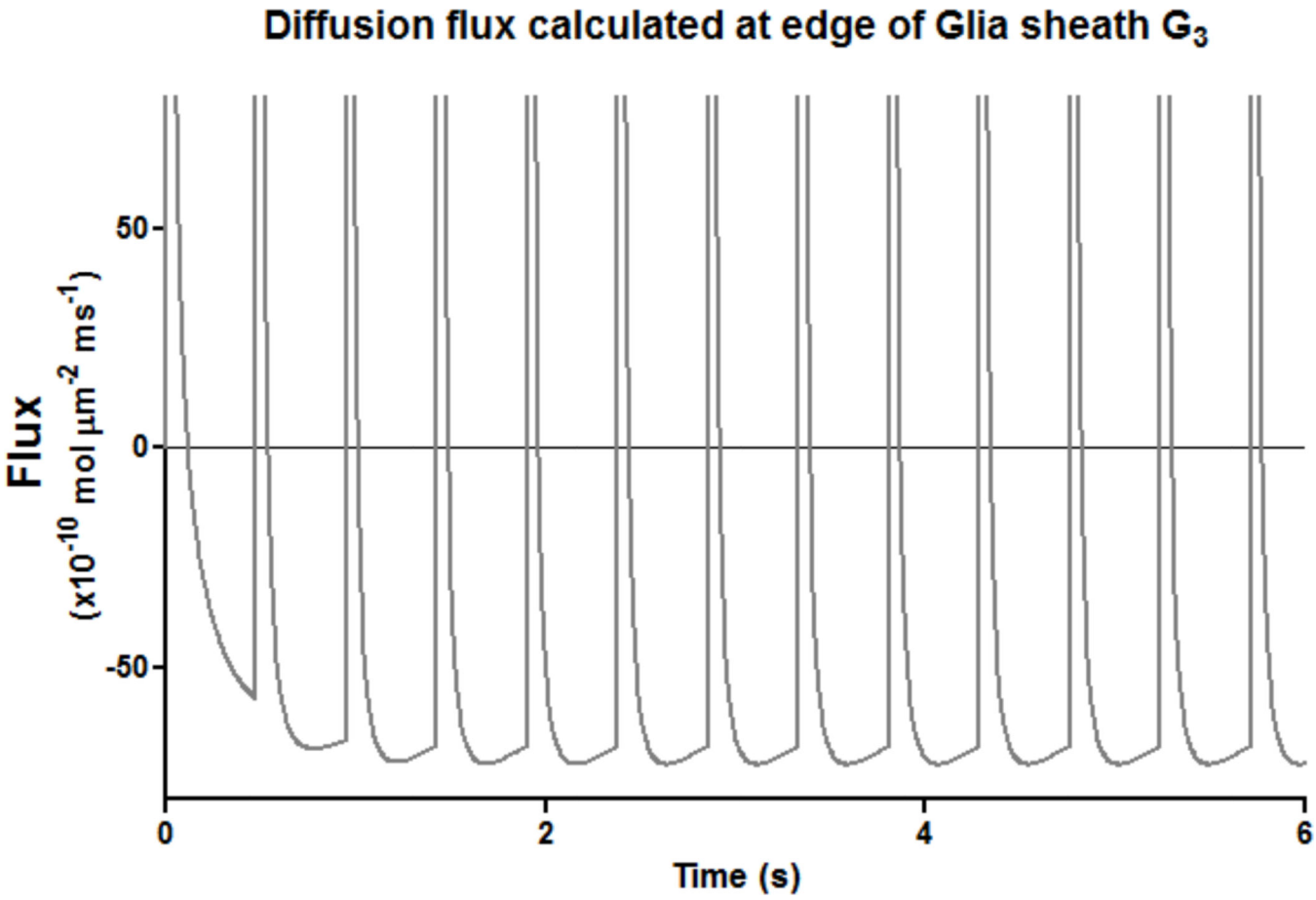

Figure 5.

Direction of glutamate flux during and after synaptic release. The flux was monitored at the edge of the outer most glial sheath G_3. An example case with 15 Hz with release probability of 0.14 is shown. Positive flux values imply flow of glutamate away from synapse, while negative values indicate glutamate flow towards synapse.

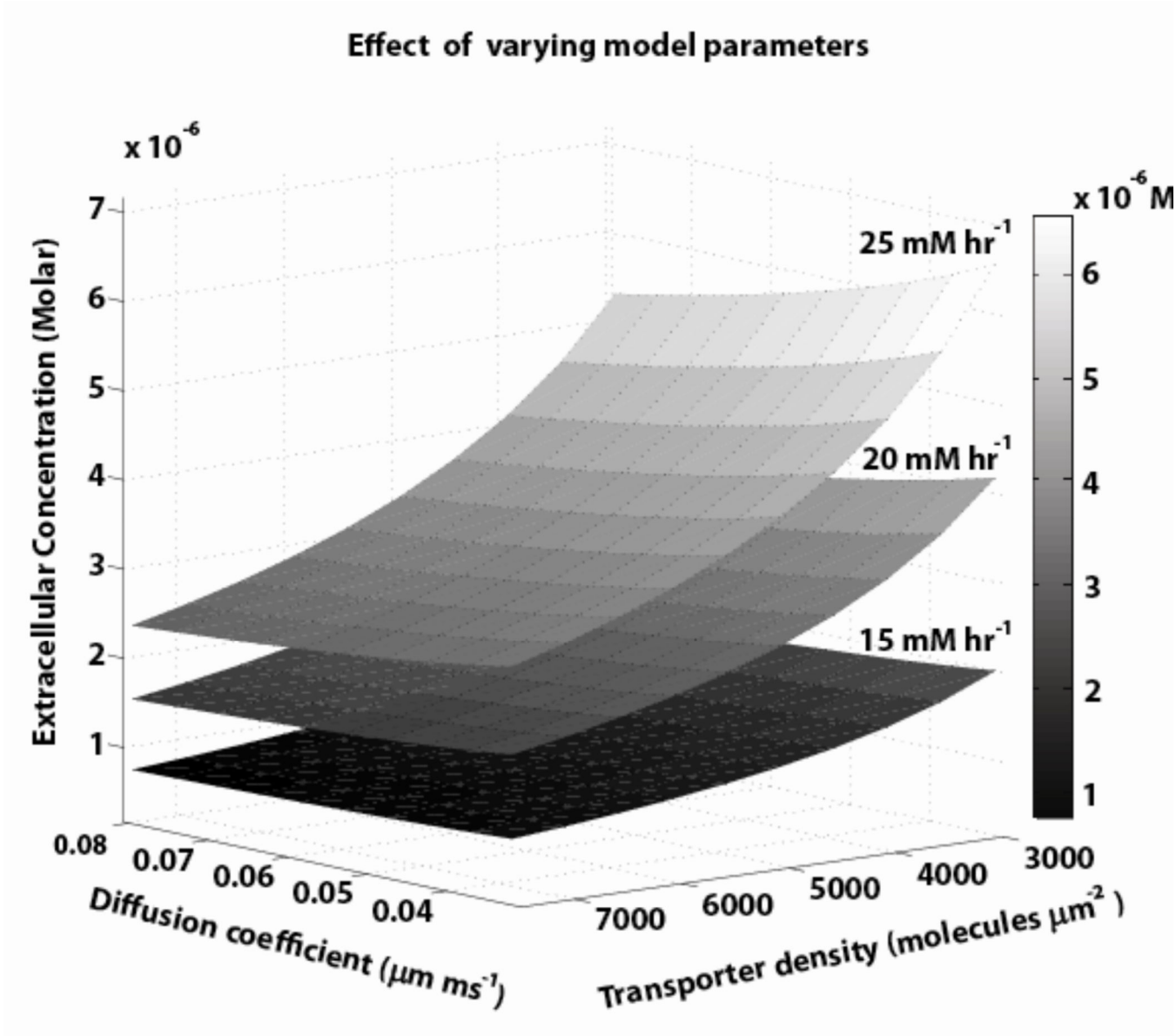

Figure 6.

Multiple parameter sets for extracellular concentrations in the range of 1–5 μM were found by concurrently varying total transporters, xc- production rate, and diffusion in the ranges shown in table 1 (the three surfaces represent three values for xc- prod rate). The other parameters were held constant at model values.

Table 1

Physiological ranges of parameters and model values for configuration 1.

Parameter	Model value	Range of values (citation)
Diffusion coefficient ($\mu m^2/ms$)	0.05	0.05 – 0.75 (Rusakov and Kullmann, 1998)
xc- prod rate (mM hr^{-1})[a]	30	10 – 55 (Wyatt et al., 1996)
Transporter Dynamics		
Total XAG (molecules)[b]	5,800	2,500 – 10,000 (Bergles and Jahr, 1997; Lehre and Danbolt, 1998)
k_1 (M^{-1} ms^{-1})	10^4	10^4 (Lehre and Rusakov, 2002)
k_{-1} (ms^{-1})	0.2	0.2 (Lehre and Rusakov, 2002)
k_2 (ms^{-1})	0.1	0.1 (Lehre and Rusakov, 2002)
Release Parameters		
No. of molecules per release	5,000	4,700 – 10,000 (Bruns and Jahn, 1995)
k_d value of mGluR 2/3 (μM)	0.187	0.1 – 0.3 (Schoepp and True, 1992)
Maximum release probability	0.4 (max)	0.1 – 0.5 (Ding et al., 2008)
Release probability used (tuned to operate near k_d Value of mGluR)	0.14 (basal)	0.12 – 0.15 (Xi et al., 2002)
Presynaptic firing frequencies		
Firing freq (Hz) (basal)	1	1 – 3 (Trantham et al., 2002; Sun and Rebec, 2006)
Firing freq (Hz) (reward seeking)	15	12 – 15 (Trantham et al., 2002; Sun and Rebec, 2006)
Geometric parameters		
Average extracellular gap (nm)	50	34 – 68 (Thorne and Nicholson, 2006)
Intersynaptic distance (μm)	1	0.5 – 1 (Rusakov, 2001)

[a] xc- was volume populated on G_{3b}.

[b] XAG was volume populated on glial sheaths G_1, G_2, and G_3 with surface density of 1,400, 1,000, and 500 molecules/μm^2 for configuration 1. Same surface density was for sheaths G_1, and G_2 in configuration 2 and 3.

Table 2

Prediction of glial configurations and parameters that support specified extracellular concentrations.

Configuration 1			
P_{ex} (extracellular concentration)	**<3 μM**	**3 – 7 μM**	**7 – 12 μM**
Diffusion coefficient (μm^2/ms)	0.13 – 0.25	0.1 – 0.15	0.05 – 0.1
xc- prod rate (mM hr^{-1})	15 – 25	10 – 50	>50
Transporter density (x10^3molecules/μm^2)[a]	1.5 – 3.5	3.5 – 7	7 – 10
Configuration 2			
P_{ex} (extracellular concentration)	**<1 μM**	**1 – 3 μM**	**3 – 5 μM**
Diffusion coefficient (μm^2/ms)	0.2 – 0.4	-	-
xc- prod rate (mM h^{-1})	5 – 15	-	-
Transporter density (x10^3molecules/μm^2)[a]	2.5 – 5	-	-
Configuration 3			
P_{ex} (extracellular concentration)	**<1 μM**	**1 – 3 μM**	**3 – 5 μM**
Diffusion coefficient (μm^2/ms)	0.1 – 0.15	0.05 – 0.1	0.053
xc- prod rate (mM hr^{-1})	20 – 30	35 – 50	50 – 75
Transporter density (x10^3molecules/μm^2)[a]	2.5 – 5	4.5 – 7	7 – 10

[a] Specifies the range of transporter densities required for glial sheaths G_1, G_2, and/or G_3 to achieve cited extracellular concentration ranges.